Polycapillary Optics Based Confocal Micro X-ray Fluorescence and X-ray Absorption Spectroscopy Setup at The European Synchrotron Radiation Facility Collaborative Research Group Dutch–Belgian Beamline, BM26A

DOI:
10.1021/acs.analchem.7b05110

Document Version
Accepted author manuscript

A polycapillary optics based confocal micro-XRF and XAS setup at ESRF CRG beamline DUBBLE, BM26A

Stephen Bauters[a], Pieter Tack[a], Jennifer Helen Rudloff-Grund[b], Dipanjan Banerjee[c], Alessandro Longo[d], Bart Vekemans[a], Wim Bras[d], Frank E Brenker[b], Roelof van Silfhout[c,e] and Laszlo Vincze[a]*

[a]XMI, Department of Chemistry, Ghent University, Krijgslaan 281 S12, Ghent, East Flanders, 9000, Belgium
[b]Geoscience Institute - Mineralogy, Goethe University, Altenhöferallee 1, Frankfurt, 60438, Germany
[c]KU Leuven, DUBBLE@ESRF, CS 40220, Grenoble, F-38043, France
[d]Netherlands Organisation for Scientific Research (NWO), DUBBLE@ESRF, CS 40220, Grenoble, F-38043, France
[e] University of Manchester, School of Electrical & Electronic Engineering, Manchester, M13 9PL, England

ABSTRACT: A novel plug-and-play setup based on polycapillary X-ray optics enables 3D confocal XRF and XAS down to 8×8×11 μm^3 (17 keV) at the ESRF CRG beamline DUBBLE, BM26A. A complete description and analytical characterization is presented, together with 2 recently performed experimental cases. In Deep Earth diamond São Luiz-Frankfurt a. Main 16, an Olivine-rich inclusion was mapped with full 3D XRF elemental imaging. The preliminary tests on an Iron Gall ink containing historical document, a letter from the court of King Philip II of Spain, reveal both the delicate nature of Iron Gall ink and the lack of Fe-Ni chemical bonding.

The Dutch-Belgian beamline (DUBBLE) X-ray Absorption Spectroscopy (XAS) branch BM26A at the European Synchrotron Radiation Facility (ESRF) in Grenoble, France, specializes in providing a flexible, multi-purpose facility to the scientific community for transmission XAS, fluorescence mode XAS, in-situ XAS, SAXS/WAXS/EXAFS combination measurements, etc.[1-3] To expand on BM26A's capabilities, a polycapillary optics based plug-and-play setup was designed to provide spatially resolved confocal XAS and XRF down to the micron scale. The complete setup is mounted on two optical breadboards that can be quickly inserted at the sample position of the beamline. Polycapillary X-ray lenses are capable of accepting up to several millimeters of X-ray beam and have a fixed focal distance independent of incoming beam energy, making them ideal tools for X-ray beam focusing in confocal XAS setups.[4-6] With the plug-and-play setup presented in this work, the conversion from macro to micro-confocal beamline can be achieved in 4 hours, less than one ESRF beam time shift (8 hours). The setup enables spatial sensitive research in the fields of corrosion science, archeology and depth resolved analysis of ion-exchanged glasses.[7-10]

In this work, an in-depth characterization of the polycapillary optics and beam line conditions relevant to confocal experiments at BM26A is presented. Two recently performed experiments highlight many of the capabilities of our confocal setup, such as 3D XRF imaging and localized µ-EXAFS, on Fe-rich inclusions in a Deep Earth diamond and on the Iron Gall ink on a rare historical document, a letter from the court of King Philip II of Spain to the archbishop of Mexico.

EXPERIMENTAL SECTION

The ESRF-CRG BM26A beamline is a bending magnet source (B = 0.4 Tesla) with 103 µrad horizontal and 1.1µrad vertical divergence.[6] The micro focus achieves an X-ray beam size down to 8×8µm^2 with an XOS (X-ray Optical Systems, NY, USA) custom designed polycapillary. (Figure 1) An H206 6-axis precision alignment system (Physik Instrumente GmbH, Karlsruhe, Germany) with c-887 hexapod controller (PI) provides the precision needed to align the polycapillary with the incoming synchrotron beam. In-house procedures

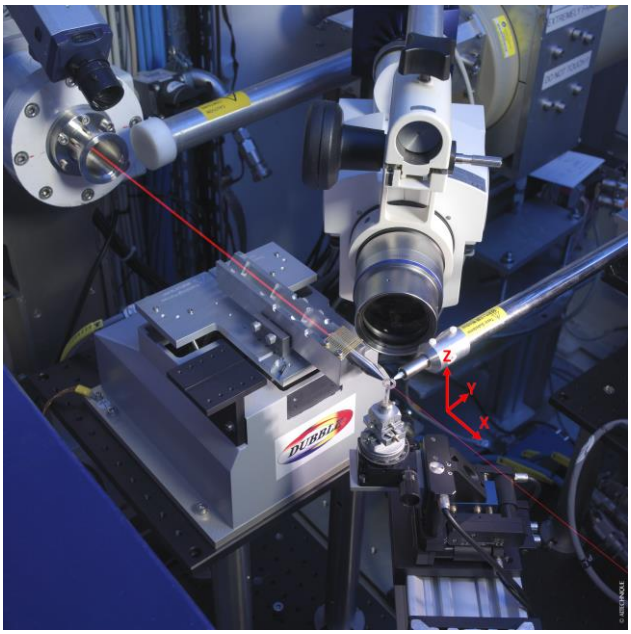

Figure 1 The confocal platform installed at beamline BM26A. The red visualization of the beam originates from the first ion chamber and passes over the H206 PI hexapod through the first XOS polycapillary optic. The Zeiss microscope coordinates placement of the stainless steel wire cross in the microbeam. A Hitachi Vortex-EM X-ray detector equiped with an XOS polycapillary optic completes the confocal volume detection scheme. Optional Dino-Lite microscopes not pictured.

written in SPEC (Certified Scientific Software, MA, USA) control software align the focusing polycapillary with minimal user-input required. A 3D confocal measuring voxel is created by limiting the field of view of the Vortex-EM (Hitachi High-Technologies Science America Inc., Japan) energy-dispersive X-ray detector with a custom-made polycapillary optic (XOS). A one channel DXP Mercury (XIA LLC, CA, USA) interprets the incoming photons with an energy resolution of 157 eV at the Cu-K fluorescence line (8.047 keV) up to 100 kcts incoming count rate. An XYZ combination of three LS-120 linear stages (PI miCos GmbH) allows for accurate detector placement with respect to the sample. A similar configuration of M-111.12S Compact Micro-Translation stages (PI), equipped with a 1005 goniometer head (HUBER Diffraktionstechnik GmbH & Co. KG, Germany), provides a flexible sample environment with micrometer resolution. Both sets of stepper motors are controlled by the ESRF ICEPAP system through SPEC. A computer-controlled SteREO Discovery V20 microscope (Carl Zeiss AG, Germany) visualizes the measured sample surface area and optionally up to two AM4815ZTL Dino-Lite (AnMo Electronics Corporation, Taiwan) handheld microscopes are available for general sample monitoring.

RESULTS AND DISCUSSION

Characteristics. *Confocal volume*. The focusing polycapillary optic was designed to accept up to 7.5×3 (Y×Z) mm^2 incoming X-ray beam, however the beam conditions at BM26A enforce an optimal incoming beam of 3×0.8 mm^2. In order to fully characterize the confocal volume dimensions, a stainless steel wire (10 µm) cross was translated throughout the microbeam. By acquiring wire scans in 1 dimension (Y or Z) at multiple positions throughout the beam (X), both the focal point at 2.5 mm from the tip of the polycapillary optic and the divergence of the beam could be accurately determined experimentally. The resulting X-ray microbeam can be defined as (Y×Z) 11×11 $µm^2$ with divergences of 4.4 and 0.4 degrees at 9.078 keV and 8 ×8 $µm^2$ with divergences of 3.1 and 0.4 degrees at 18.048 keV, as shown in Figure 2 & 3. The X dimension of the confocal volume is defined by the polycapillary optic mounted on the fluorescence detector. By utilizing the Fe-fluorescence from the wire as secondary X-ray source, an X dimension of 12 µm at 9.078 keV and 11 µm at 18.048 keV was measured by scanning the fluorescence detector in the X direction.

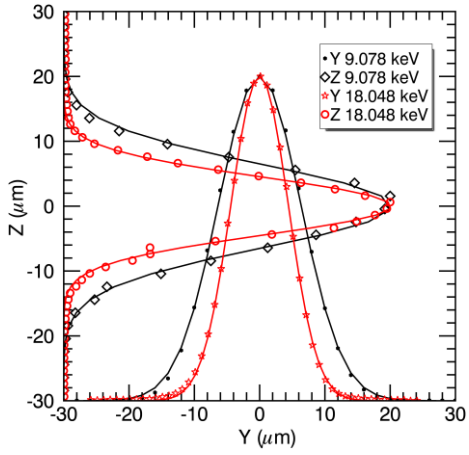

Figure 2 Results of wire scans performed at the focal position with fitted Gaussians as solid line, visualizing the (Y×Z) 8×8 $µm^2$ beam at 18.048 keV and 11×11 $µm^2$ beam at 9.078 keV. Fluorescence intensities are plotted in arbitrary units for comparison.

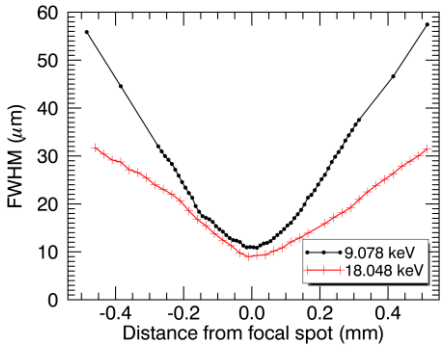

Figure 3 Visualization of the beam size, determined with the wire scan method, at different positions relative to the optimal focal distance, showing a horizontal divergence of 4.4 degrees at 9.078 keV and 3.1 degrees at 18.046 keV.

Detection limits. The XRF Limits of Detection (LoD) for the confocal mode were determined with a pellet pressed from the NIST Standard Reference Material 1577c bovine liver powder, measured for 1000 seconds at 9 and 18 keV. (Figure 4)

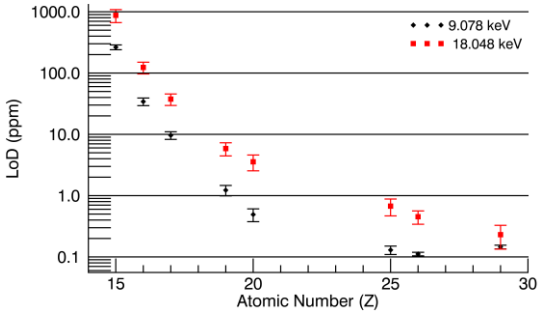

Figure 4 Limits of detection limits for a NIST SRM1577c bovine liver pellet, 1000s real time at 3% dead time.

Transmission efficiency. By quantifying the photon flux before and after the focusing polycapillary optic using Oxford ionization chambers, a clear decreasing trend for the transmission efficiency (ε) of the polycapillary as a function of photon energy is evident in Figure 5. This leads to an intensity gain factor (G) of minimum 16000, due to the small focus achieved, as calculated by[5]

$$G = \varepsilon \frac{S_{input}}{S_{focus}}$$

with S being the surface area of the beam at the polycapillary optic entrance and at the focus.

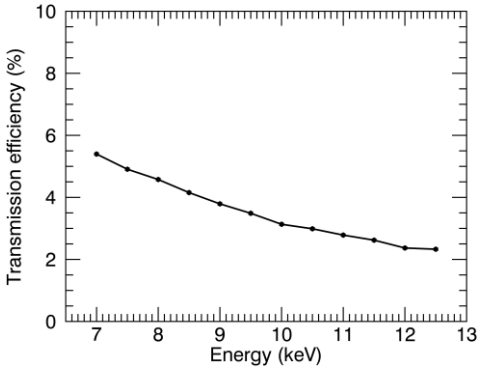

Figure 5 Transmission efficiency of the polycapillary focusing lens in the typical transmission metal range as a function of photon energy.

Experimental case I: Deep Earth diamond

The investigated Deep Earth diamond originates from depths down to the lower mantle (>660 km) and were excavated from the São-Luiz alluvial diamond deposit in the Juina area, Mato Grosso State, Brazil. During their formation, these type of diamonds can encapsulate material and become chemical resistant sample carriers from the Earth's mantle transitions zone, becoming vital composition information probes.[11-15] To preserve the chemical conditions inside the inclusions, it is preferred to assess the composition without physically damaging the diamonds. Confocal XRF and XAS are ideal analytical techniques for this requirement, because the X-rays can easily penetrate the carbon diamond material whilst the confocal configuration minimizes carbon scatter detection and thus detector overload. All XRF mappings were performed at 7.21 keV and with a 20 µm step size for 2D and 5 µm step size in 3D mapping and 1 s dwell time. XANES point measurements were done from 7.042 keV to 7.210 keV and processed with in-house developed IDL software for linear combination analysis (LCA).

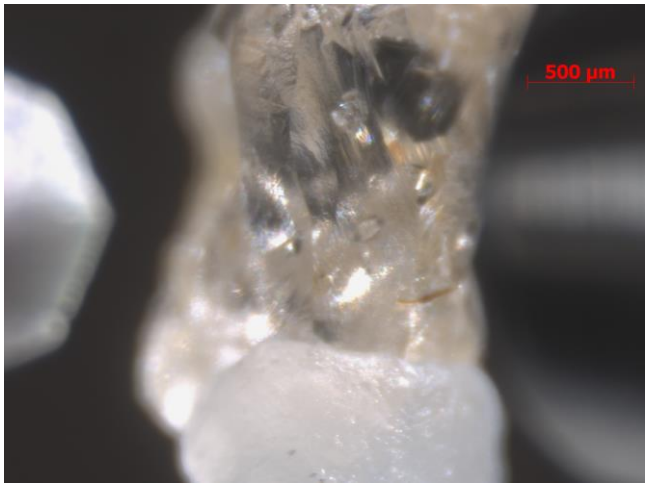

Figure 6 Diamond São Luiz-Frankfurt a. Main (SL-FFM) 16 at sample position as seen with the Zeiss optical microscope. Both the focusing as detector polycapillary optics can be seen on the right and left respectively.

A 1.5×0.7 mm^2 2D mapping was done on diamond SL-FFM 16 (Figure 6) to confirm the placement of the inclusion in the X-ray beam and to locate any possible invisible inclusions. (Figure 7) LCA of the XANES spectrum combining to up to 8 different Fe standards and minerals reveals a predominantly Olivine presence of 91% together with 9% Fe_2O_3. (Figure 8)

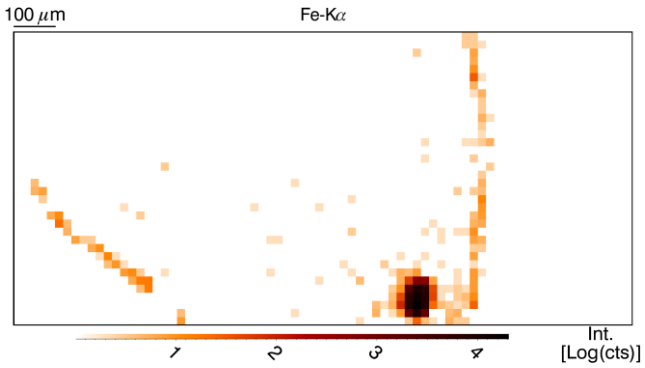

Figure 7 Fe-Kα elemental XRF spatially resolved image of the area around the investigated Fe-rich inclusion in the SL-FFM 16 diamond.

To display the 3D capabilities of the confocal setup, a 170×170×70 µm^3 XRF mapping was performed on a different inclusion. Data processing in IDL was straight forward, as all spectra relate to a specific spatial voxel with known motor positions, and can be a powerful elemental visualization tool. (supplement movie 1)

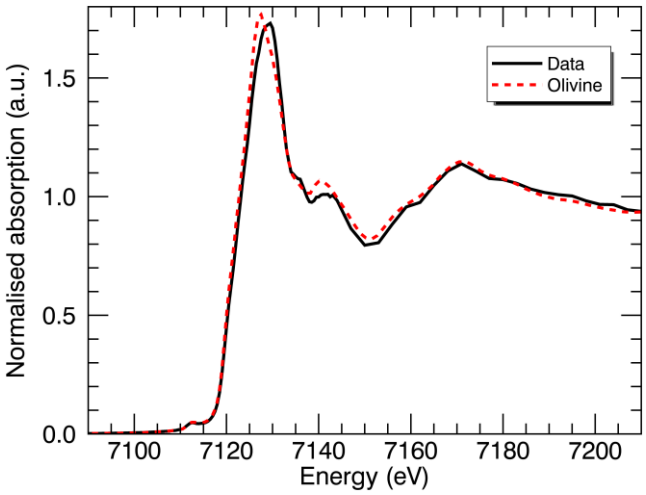

Figure 8 XANES profile of an SL-FFM 16 Fe-rich inclusion (black) compared to an Olivine (red) reference spectrum. X-ray voxel size 16×14×13 µm^3 with 1 s dwell time per point.

Experimental case II: Iron Gall ink

Preliminary tests were done on Iron Gall ink in a letter originating from the court of King Philip II of Spain addressed to the archbishop of Mexico, to assess the degradation of the historical document and to attempt to geographically trace the original Fe:Ni containing ores used to produce the Iron Gall ink.[16-18] (Figure 9) To detect any possible inhomogeneity of the ink and paper, a 3.5×2.25 mm^2 2D elemental mapping with 20 µm resolution at 8.5 keV was performed. (Figure 10) Based on the elemental images, quantified with the fundamental parameter method and a NIST SRM 1577c bovine liver standard[19], representative spots of paper (a) and Iron Gall ink (b) were investigated by Fe-K edge XAS up to a 7.261 keV for XANES and up to a k value of 12 (7.656 keV) for EXAFS analysis with VIPER[20] and FEFF9[21].

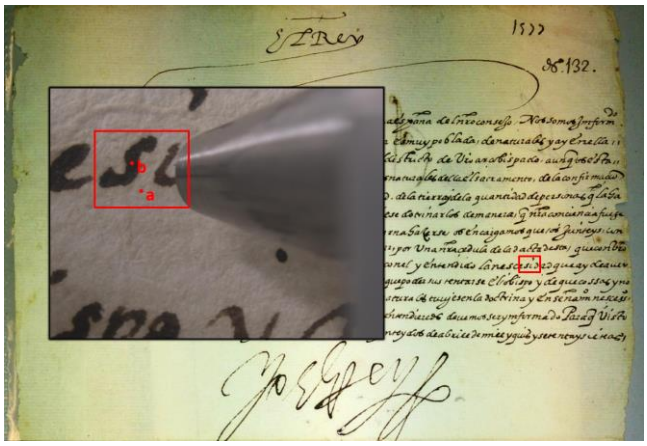

Figure 9 The Iron Gall ink(a) and paper(b) from a letter of the court King Philip II of Spain were mapped by XRF spectroscopy and further analysed in detail by point XAS measurements.

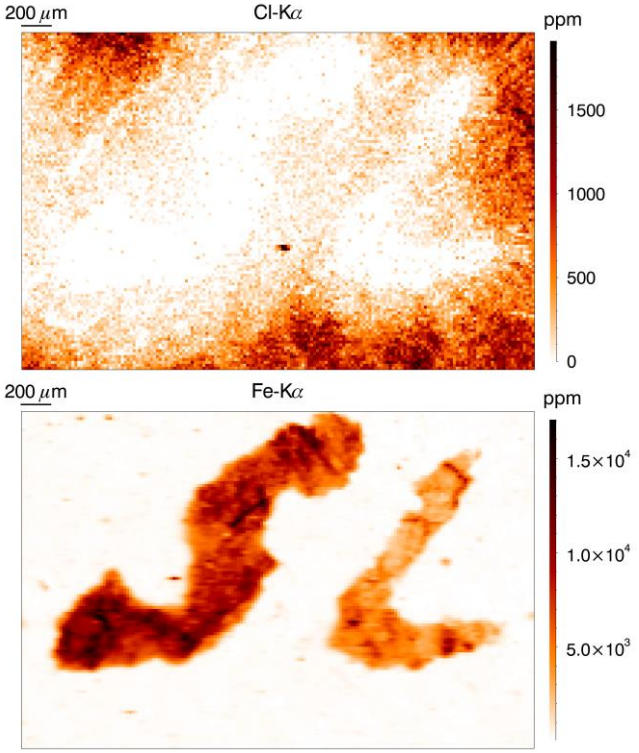

Figure 10 Elemental XRF images (Cl and Fe) of the 3.5×2.25 mm^2 mapping of Iron Gall ink letters on paper.

The lack of a strong pre-edge peak in the EXAFS spectrum suggests a symmetrical octahedral direct coordination of the Fe atoms, which is confirmed by the EXAFS first shell fit, typical for Iron Gall ink.[17] (Figure 11) The presence of any Fe-Ni interaction up until the 3rd shell is not detected. This could indicate that the original ore used to produce the Iron Gall ink did not contain any Ni and that the presence of Ni in the ink has to be explained in another way. Further investigation is required, but one can speculate that the Ni was added, either accidentally or on purpose, during the manufacturing process. Also typical in this process, vitriol solution (FeSO4) is extracted from the original ores, a chemically mobile and unbound form of Fe, removing any chemical correlation with potentially present Ni.[22-24]

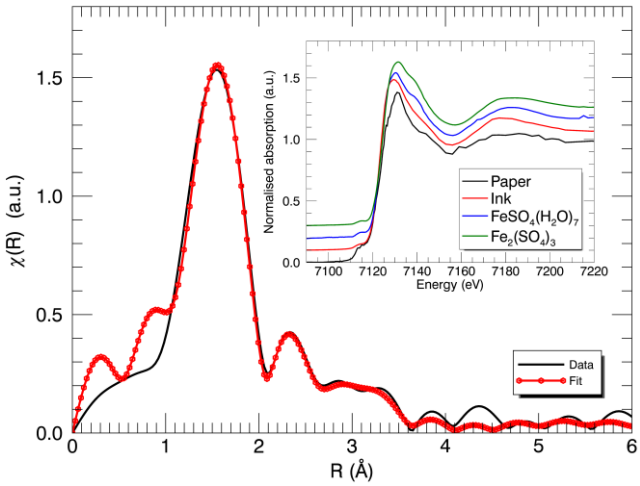

Figure 11 XANES(inset) profiles of the Iron Gall ink(red [+0.1]), paper(black) and octohedral iron sulphate standards (iron(II) blue [+0.2] and iron(III) green [+0.3]). The main graph shows the EXAFS pseudo radial distribution magnitude of the ink(black) and the fit(red) using FEFF9.

Although the Fe:Ni ratio is interesting in the search for provenance of the original iron in the ink for conservation purposes, it is known that the ratio of Fe^{2+} and Fe^{3+} is a good indicator for the degree of potential degradation, ie. the ability for chemical degradation to still occur, of the Iron Gall ink for paper due to the depletion of Fe^{3+} in the degradation process.[22,24] Figure 12 shows however that repeated XANES measurements expose the ink with too high doses of X-rays, causing the formation of Fe^{2+} and thus increasing the potential degradation damage. This form of radiation influence is becoming more prevalent with the use of microfocus and high intensity beamlines[25].We are at the moment investigating the possibility to perform Quick-EXAFS experiments at BM26A to counter-act this problem for future Iron Gall research on a rare historical map of the American continent, the *Tabula Moderna alterius hemisphaerii*.

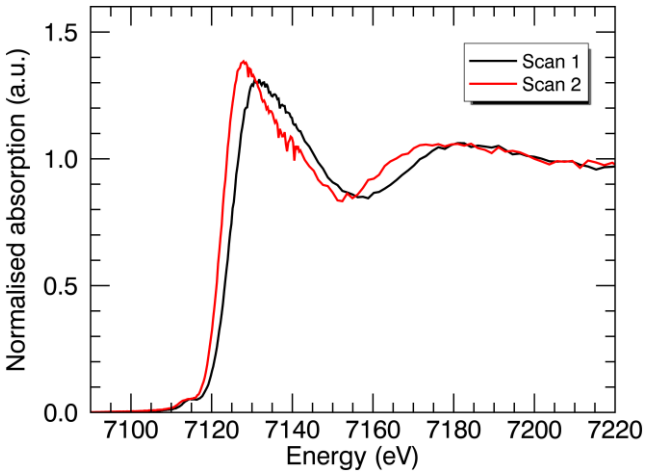

Figure 12 Two consecutive XANES scans on the same Iron Gall ink spot. A clear edge energy shift indicates a higher presence of Fe^{2+}. Total exposure time per scan was 122 s with an estimated beam intensity of 1.4×10^9 photons/s in the confocal volume.

CONCLUSIONS

The analytical characterization of the novel polycapillary based plug-and-play confocal setup for micro XRF and XAS at the ESRF CRG beam line DUBBLE, BM26A was demonstrated. An achieved beam focus of 8×8 μm^2, intensity gain factors of 16000+ and detection limits to sub-ppm levels allow for a whole range of new spatially resolved research. A first experiment on a Deep Earth diamond Fe-rich inclusion demonstrates the powerful elemental imaging capabilities by full 3D mapping. A second experimental case shows the feasibility of XANES and EXAFS on an Iron Gall ink sample whilst confirming the X-ray sensitive nature of the material.

ASSOCIATED CONTENT

Supporting Information

Supplement movie 1: 3D visualization of an elemental XRF mapping on an Fe-rich inclusion in Deep Earth diamond SL-FFM 16

Corresponding Author

* Email: Laszlo.Vincze@ugent.be

Author Contributions

The manuscript was written through contributions of all authors.

ACKNOWLEDGMENTS

We would like to acknowledge Frederik Muller for providing the letter originating from the court of King Philip II of Spain and Daniel Michon (Artechnique) for the professional photoshoot of the setup as seen in figure 1. Dirk Detollenaere and Florian Ledrappier from the DUBBLE beamline are thanked for their extensive support during development and construction.

REFERENCES

(1) Borsboom, M.; Bras, W.; Cerjak, I.; Detollenaere, D.; van Loon, D.; Goedtkindt, P.; Konijnenburg, M.; Lassing, P.; Levine, Y.; Munneke, B.; Oversluizen, M.; van Tol, R.; Vlieg, E. *Journal of Synchrotron Radiation* **1998**, 5, 518-520.

(2) Nikitenko, S.; Beale, A.; van der Eerden, A.; Jacques, S.; Leynaud, O.; O'Brien, M.; Detollenaere, D.; Kaptein, R.; Weckhuysen, B.; Bras, W. *Journal of Synchrotron Radiation* **2008**, 15, 632-640.

(3) Meire, M.; Tack, P.; De Keukeleere, K.; Balcaen, L.; Pollefeyt, G.; Vanhaecke, F.; Vincze, L.; Van Der Voort, P.; Van Driessche, I.; Lommens, P. *Spectrochimica Acta Part B-Atomic Spectroscopy* **2015**, *110*, 45-50.

(4) Vincze, L.; Wei, F.; Proost, K.; Vekemans, B.; Janssens, K.; He, Y.; Yan, Y.; Falkenberg, G. *Journal of Analytical Atomic Spectrometry* **2002**, *17*, 177-182.

(5) Silversmit, G.; Vekemans, B.; Nikitenko, S.; Bras, W.; Czhech, V.; Zaray, G.; Szaloki, I.; Vincze, L. *Journal of Synchrotron Radiation* **2009**, *16*, 237-246.

(6) Silversmit, G.; Vekemans, B.; Nikitenko, S.; Schmitz, S.; Schoonjans, T.; Brenker, F.; Vincze, L. *Physical Chemistry Chemical Physics* **2010**, *12*, 5653-5659.

(7) Grieten, E.; Schalm, O.; Tack, P.; Bauters, S.; Storme, P.; Gauquelin, N.; Caen, J.; Patelli, A.; Vincze, L.; Schryvers, D. *Journal of Cultural Heritage* **2017**.

(8) Schalm, O.; Crabbe, A.; Storme, P.; Wiesinger, R.; Gambirasi, A.; Grieten, E.; Tack, P.; Bauters, S.; Kleber, C.; Favaro, M.; Schryvers, D.; Vincze, L.; Terryn, H.; Patelli, A. *Applied Physics a-Materials Science & Processing* **2016**, *122*.

(9) Tack, P.; Bauters, S.; Mauro, J. C.; Smedskjaer, M. M.; Vekemans, B.; Banerjee, D.; Bras, W.; Vincze, L. *Rsc Advances* **2016**, *6*, 24060-24065.

(10) Tack, P.; Cotte, M.; Bauters, S.; Brun, E.; Banerjee, D.; Bras, W.; Ferrero, C.; Delattre, D.; Mocella, V.; Vincze, L. *Scientific Reports* **2016**, *6*.

(11) Brenker, F.; Vollmer, C.; Vincze, L.; Vekemans, B.; Szymanski, A.; Janssens, K.; Szaloki, I.; Nasdala, L.; Joswig, W.; Kaminsky, F. *Earth and Planetary Science Letters* **2007**, 260, 1-9.

(12) Kaminsky, F.; Zakharchenko, O.; Davies, R.; Griffin, W.; Khachatryan-Blinova, G.; Shiryaev, A. *Contributions To Mineralogy and Petrology* **2001**, 140, 734-753.

(13) Harte, B.; Harris J.W. *Mineral Mag* 1994, 58A, 384-385.

(14) Pearson, D.; Brenker, F.; Nestola, F.; McNeill, J.; Nasdala, L.; Hutchison, M.; Matveev, S.; Mather, K.; Silversmit, G.; Schmitz, S.; Vekemans, B.; Vincze, L. *Nature* **2014**, 507, 221-+.

(15) Silversmit, G.; Vekemans, B.; Appel, K.; Schmitz, S.; Schoonjans, T.; Brenker, F.; Kaminsky, F.; Vincze, L. *Analytical Chemistry* **2011**, *83*, 6294-6299.

(16) Hahn, O.; Malzer, W.; Kanngiesser, B.; Beckhoff, B. *X-Ray Spectrometry* **2004**, 33, 234-239.

(17) Proost, K.; Janssens, K.; Wagner, B.; Bulska, E.; Schreiner, M. *Nuclear Instruments & Methods in Physics Research Section B-Beam Interactions With Materials and Atoms* **2004**, 213, 723-728.

(18) Wilke, M.; Hahn, O.; Woodland, A.; Rickers, K. *Journal of Analytical Atomic Spectrometry* **2009**, 24, 1364-1372.

(19) Schoonjans, T.; Silversmit, G.; Vekemans, B.; Schmitz, S.; Burghammer, M.; Riekel, C.; Brenker, F. E.; Vincze, L. *Spectrochimica Acta Part B-Atomic Spectroscopy* **2012**, *67*, 32-42

(20) Klementev, K. *Journal of Physics D-Applied Physics* **2001**, 34, 209-217.

(21) Rehr, J.; Kas, J.; Vila, F.; Prange, M.; Jorissen, K. *Physical Chemistry Chemical Physics* **2010**, 12, 5503-5513

(22) Poggi, G.; Giorgi, R.; Toccafondi, N.; Katzur, V.; Baglioni, P. *Langmuir* **2010**, *26*, 19084-19090.

(23) Smith, C.S.; Gnudi, M.T. *The Pirotechnia of Vannoccio Biringuccio* **1943**, 95-97

(24) Kurouski, D.; Zaleski, S.; Casadio, F.; Van Duyne, R.; Shah, N. *Journal of the American Chemical Society* **2014**, 136, 8677-8684.

(25) Bras, W.; Stanley, H. *Journal of Non-Crystalline Solids* **2016**, 451, 153-160.

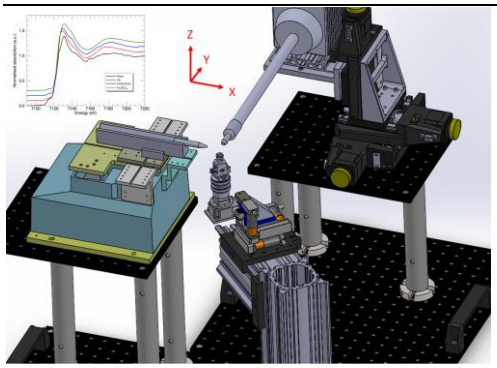

for TOC

Keywords: *micro-XRF, micro-XAS, polycapillary optics, Iron Gall ink, Deep Earth diamond*